Capacity Approaching Codes for Non-Coherent Orthogonal Modulation

Albert Guillén i Fàbregas, *Member, IEEE* , and Alex J. Grant, *Senior Member, IEEE*

***Abstract*— This paper describes a curve-fitting approach for the design of capacity approaching coded modulation for orthogonal signal sets with non-coherent detection. In particular, bit-interleaved coded modulation with iterative decoding is considered. Decoder metrics are developed that do not require the knowledge of the signal-to-noise ratio, yet still offer very good performance.**

***Index Terms*— Belief propagation (BP), bit-interleaved coded modulation (BICM), channel capacity, decoding threshold, density evolution, extrinsic information, iterative decoding, non-coherent frequency-shift keying (NFSK), orthogonal modulation, repeat-accumulate codes, turbo codes.**

I. Introduction

Orthogonal modulation with non-coherent detection is a practical choice for situations where the received signal phase cannot be reliably estimated and/or tracked. There are many important applications where this is the case. Examples include military communications using fast frequency hopping, airborne communications with high Doppler shifts due to significant relative motion of the transmitter and receiver, and high phase noise scenarios, due to the use of inexpensive or unreliable local oscillators.

A common choice of implementation for the modulator is frequency shift keying (FSK), and in the remainder of the paper we will therefore refer to non-coherent FSK (NC-FSK).

Capacity analysis of M-ary NC-FSK [1] reveals a trade-off between the modulation order M and the minimum energy per bit E_b required for reliable communications. Increasing M reduces the required E_b. This is useful in cases where transmit power is more important than spectral efficiency, such as low probability of intercept communications.

It is therefore of some interest to consider the design of error control codes which approach the capacity of these non-coherent channels. In the literature, concatenations of Reed Solomon (RS) codes and convolutional codes have been considered [2], as well as RS codes combined with repeat diversity [3], [4], [5]. Trellis coded modulation has been considered in [6]. The use of turbo codes has been considered in [7], [8], where the capacity of the binary NC-FSK channel was approached within about 0.7 dB on Rayleigh fading channels. As discussed above however, higher order modulation may be of more interest.

More recently, bit interleaved coded modulation with iterative decoding (BICM-ID) [9], [10] has been considered for the NC-FSK channel [11], [12], [13]. Using the standard cdma2000 turbo code with rates $1/2$, $1/3$, $1/4$ and $1/5$ they report simulation results ranging from about 0.9 dB from capacity for 4-ary NC-FSK to about 1.7 dB from capacity for 64-ary NC-FSK (with Rayleigh fading). Although a gain is demonstrated by iterating between demodulation and decoding, no optimization of the component codes is considered.

Another important consideration in many applications is the amount of channel state information (CSI) available at the decoder. This may range from full CSI, where the decoder knows the instantaneous fading amplitude and the average signal-to-noise ratio (SNR), to partial CSI, where only the average SNR is known, right through to no CSI, where not even the SNR is known. The latter case is of interest for partial band jamming of a fast frequency hopped system, where the resulting SNRs for each of the M frequency bins may vary with frequency and time. Valenti and Cheng [13] develop decoder metrics for both the full and partial CSI scenarios, but do not consider the complete absence of CSI.

There are two main contributions in this paper. First, in Section IV, we develop low-complexity decoder metrics suitable for iterative decoding/demodulation with no CSI. We demonstrate the corresponding effect of loss of CSI on the extrinsic information (EXIT) charts [14] of the demodulator. Secondly, in Section V we use curve fitting of EXIT charts [15], [16] to optimize the degree sequences for outer irregular repeat-accumulate codes [17] for use with an inner rate-1 recursive M-ary modulator. The resulting codes outperform all previously reported results for the NC-FSK channel.

Notation: All vectors will be column vectors, and will be denoted using bold face, e.g. $\mathbf{x} = (x_0, x_1, \ldots, x_{n-1})^T \in \mathbb{C}^n$ is a column vector with n complex elements. $\mathcal{N}\left(\mu, \sigma^2\right)$ denotes the circularly symmetric complex Gaussian density, with mean μ and variance $\sigma^2/2$ in the real and imaginary components. $|\cdot|$ denotes the magnitude of its complex argument. The relationship $a \propto b$ is used to denote that quantity a is proportional to quantity b.

II. System Model

We assume that the modulation order is a power of two, $M = 2^m$, where m is an integer $m \geq 1$. With reference to Figure 1, an information source produces a binary sequence

A. Guillén i Fàbregas was with the Institute for Telecommunications Research, University of South Australia, Mawson Lakes SA 5095, Australia. He is now with the Department of Engineering, University of Cambridge, Trumpington Street, Cambridge, CB2 1PZ, UK, (e-mail: guillen@ieee.org).

A. J. Grant is with the Institute for Telecommunications Research, University of South Australia, Mawson Lakes SA 5095, Australia, (e-mail: alex.grant@unisa.edu.au).

This work has been supported by the Australian Research Council (ARC) Grants DP0344856 and DP0558861.

$u[i]$, $i = 0, 1, \ldots, RLm - 1$, which is encoded at rate R to produce the binary sequence $c[j]$, $j = 0, 1, \ldots, Lm-1$, where L is an integer. The coded bit sequence is bit-wise permuted, resulting in $c[\pi(j)]$.

The output of the M-FSK modulator is a sequence of M-vectors $\mathbf{x}[k]$, $k = 0, 1, \ldots, L-1$. Each element $x_b[k]$ of this vector corresponds to one of the M frequency bins. Hence each vector $\mathbf{x}[k]$ is all zeros, except for a single element $x_b[k] = 1$, corresponding to transmission on a particular frequency bin $b \in \{0, 1, \ldots, M-1\}$ at time k. The output alphabet of the modulator is therefore $\mathcal{E} = \{\mathbf{e}_b : b = 0, 1, \ldots, M-1\}$, where $\mathbf{e}_b$ is the canonical basis vector with a one at position b and zeros everywhere else.

For the moment we leave the precise modulation mapping $\{0,1\}^m \to \mathcal{E}$ unspecified. A memoryless modulator performs a natural mapping of consecutive blocks of m bits from $c[j]$. Alternatively, the modulator could have memory (e.g. a rate 1 recursive trellis code).

The channel output at symbol time k is given by

$$\mathbf{y}[k] = \sqrt{E_s} h[k] \mathbf{x}[k] + \mathbf{n}[k]$$

where E_s is the per-symbol transmit power, $h[k] \in \mathbb{C}$ is the channel gain at time k and $\mathbf{n}[k] \sim \mathcal{N}(0, N_0)$ is a vector of zero-mean circularly symmetric complex Gaussian noise samples, with variance N_0.

Setting $h[k] = 1$ for $k = 0, 1, \ldots, L-1$, results in an additive white Gaussian noise (AWGN) channel. Fast, flat fading is modeled by letting $h[k] \sim \mathcal{N}(0, 1)$, or in polar coordinates, $h[k] = a[k] e^{i\theta[k]}$ with $a[k]$ i.i.d. Rayleigh and $\theta[k]$ uniform over $[0, 2\pi)$. Thus under either channel model, the average SNR is $\gamma \triangleq E_\mathrm{s}/N_0$, while for the Rayleigh channel, the instantaneous SNR is $a^2[k]\,\gamma$. The energy per source bit is $E_\mathrm{b} = E_\mathrm{s}/(Rm)$.

Where it causes no confusion, we will omit the symbol time indexing k.

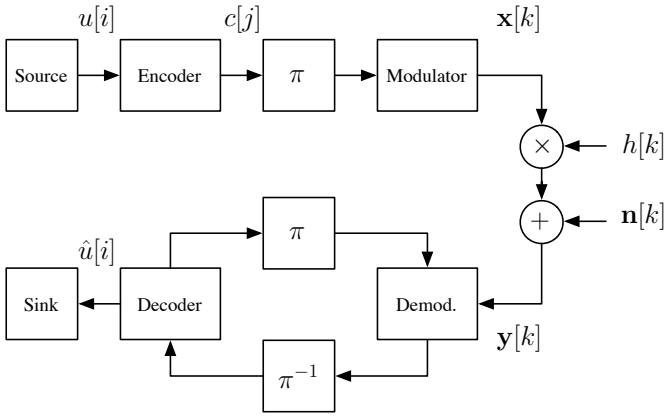

Fig. 1. System model.

A non-coherent receiver simply measures the energy $|y_b|^2$ of each frequency bin, and the resulting channel transition probabilities are given by [18]

$$p(\mathbf{y} \mid \mathbf{x} = \mathbf{e}_b) = K I_0\left(2\frac{\sqrt{E_\mathrm{s}}}{N_0} a |y_b|\right) \tag{1}$$

where the normalization constant

$$K = \frac{1}{(\pi N_0)^M}\, e^{-\frac{1}{N_0}\left(E_\mathrm{s} a^2 + \|\mathbf{y}\|^2\right)}$$

is independent of the hypothesis b, and $I_0(.)$ is the zeroth order modified Bessel function of the first kind [19]. Note that the transition probabilities depend on the ratio $a\sqrt{E_\mathrm{s}}/N_0$ rather than the ratio $a^2\,\gamma$ appearing in coherent detection.

The transition probabilities in (1) can be very easily evaluated with extremely high precision and low-complexity using with the algorithm presented in [20] based on the polynomial expansions of [19].

III. Channel Capacity

The channel capacity of the non-coherent FSK channel was found by Stark in [1] and is given by,

$$C = \log_2 M - \mathbb{E}_{\mathbf{y}|\mathbf{x}=\mathbf{e}_0}\left[\log_2\left(1 + \sum_{b=1}^{M-1} \Lambda_b(\mathbf{y})\right)\right] \tag{2}$$

where

$$\Lambda_b(\mathbf{y}) = \frac{I_0\left(2\frac{\sqrt{E_\mathrm{s}}}{N_0} a |y_b|\right)}{I_0\left(2\frac{\sqrt{E_\mathrm{s}}}{N_0} a |y_0|\right)}. \tag{3}$$

Figure 2 shows the minimum E_b/N_0 (in dB) required for reliable communication with M-FSK with non-coherent detection in AWGN and Rayleigh fading (solid lines), for $M = 4, 8, 16, 64$. There are two main observations. First, increasing the bandwidth (increasing M) reduces the required E_b/N_0. Secondly, in contrast to the coherent channel, as the code rate $R \to 0$, the required $E_\mathrm{b}/N_0 \to \infty$. Thus there is a non-trivial rate which optimizes the required E_b/N_0 for any given M.

In the case where non-optimal metrics are used, the *mismatched* mutual information [21], [22] is given by [1]

$$I^\star(X;Y) = \log_2 M - \mathbb{E}_{\mathbf{y}|\mathbf{x}=\mathbf{e}_0}\left[\log_2\left(1 + \sum_{b=1}^{M-1} \Lambda_b^\star(\mathbf{y})\right)\right] \tag{4}$$

where

$$\Lambda_b^\star(\mathbf{y}) = \frac{p^\star(\mathbf{y} \mid \mathbf{x} = \mathbf{e}_b)}{p^\star(\mathbf{y} \mid \mathbf{x} = \mathbf{e}_0)} \tag{5}$$

and $p^\star(\mathbf{y} \mid \mathbf{x} = \mathbf{e}_b)$ are the transition probabilities used by the decoder. Note that if $p^\star(\mathbf{y} \mid \mathbf{x} = \mathbf{e}_b) = p(\mathbf{y} \mid \mathbf{x} = \mathbf{e}_b)$ we have that $I^\star(X;Y) = C$.

IV. Metrics for Iterative Decoding

Iterative decoding of BICM [9], [10] has shown promise for the NC-FSK channel [13]. The main idea is to iterate between soft demodulation and soft decoding, as shown in Figure 1. Gains of 0.7 to 1 dB have been reported compared to single-pass decoding of BICM.

In this section we will develop metrics suitable for use in such decoders. There are two main design objectives. First, the metrics should have a simple implementation. Secondly,

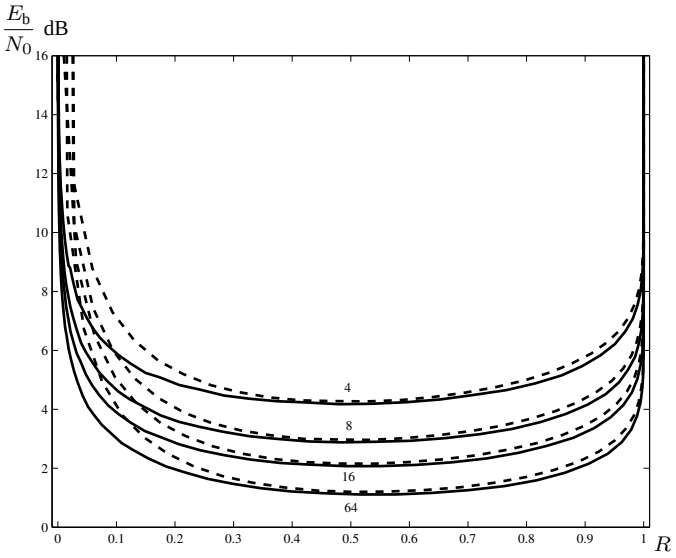

(a) AWGN channel.

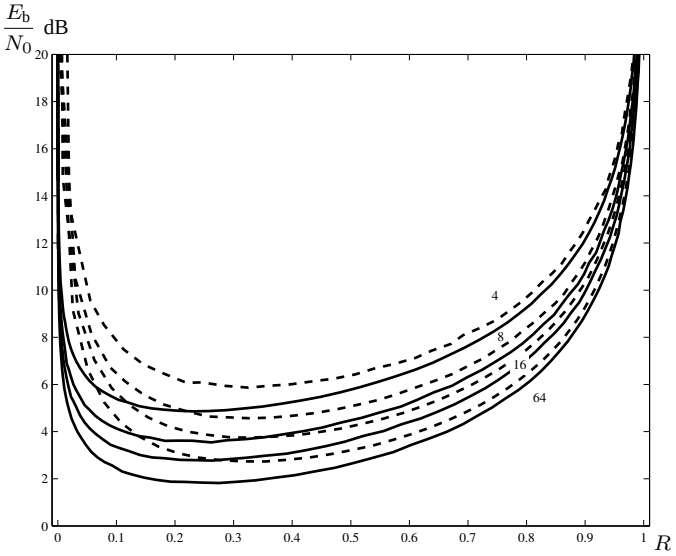

(b) Rayleigh fading AWGN channel.

Fig. 2. Minimum E_b/N_0 versus code rate R required for reliable communication with M-ary FSK with non-coherent detection in AWGN for $M = 4, 8, 16, 64$. Solid lines correspond to the channel capacity (2) and dashed lines correspond to the parameter free mutual information (15).

it is desirable to develop metrics that do not require any CSI, i.e. do not depend on $a[k]$, E_s and N_0.

A memoryless NC-FSK modulator transmits $\mathbf{x}[k] = \mathbf{e}_b$ at symbol time k where the active frequency bin b is according to

$$b = \sum_{i=0}^{m-1} c[j(k,i)]\, 2^i.$$

where $j(k,i) = \pi^{-1}(mk+i)$, $i = 0, 1, \ldots, M-1$ are the indexes of the m coded bits modulated into symbol k.

Let $\mathcal{B}_0^i \subset \{0, 1, \ldots, M-1\}$ and $\mathcal{B}_1^i \subset \{0, 1, \ldots, M-1\}$ denote the sets of indexes with a zero or a one in the i-th position of their binary representation, respectively.

For $b \in \{0, 1, \ldots, M-1\}$, $k \in \{1, 2, \ldots, L-1\}$ and $i \in \{0, 1, \ldots, m-1\}$, define the extrinsic probabilities [24]

$$q_{k,i}(b) = \prod_{\substack{l=0 \\ l \neq i}}^{m-1} \Pr\left(c[j(k,l)] = b\right).$$

Standard iterative BICM demodulation [9] consists of feeding the decoder with the following metrics (in log-likelihood ratio form)

$$\begin{aligned}\mathcal{L}(c[j(k,i)]) &= \log \frac{p(c[j(k,i)]=0)}{p(c[j(k,i)]=1)} \\ &= \log \frac{\sum_{b \in \mathcal{B}_0^i} p\left(\mathbf{y}[k] \mid \mathbf{e}_b\right) q_{k,i}(b)}{\sum_{b \in \mathcal{B}_1^i} p\left(\mathbf{y}[k] \mid \mathbf{e}_b\right) q_{k,i}(b)}. \end{aligned} \quad (6)$$

Substituting (1) into (6), we obtain the iterative decoder used by [13].

The summations in (6) may be undesirable from the point of view of complexity. To avoid these summations, the log likelihood ratio (6) may be approximated in the following standard way

$$\begin{aligned}\mathcal{L}(c[j(k,i)]) \approx &\max_{b \in \mathcal{B}_0^i} \log \left[I_0\left(2\frac{\sqrt{E_s}}{N_0} a[k]\, |y_b[k]|\right) q_{k,i}(b)\right] \\ &- \max_{b \in \mathcal{B}_1^i} \log \left[I_0\left(2\frac{\sqrt{E_s}}{N_0} a[k]\, |y_b[k]|\right) q_{k,i}(b)\right] \end{aligned} \quad (7)$$

We shall refer to (6) and (7) as the Bessel and Bessel dual-max metrics respectively.

Note that in order to compute (6) and (7), the signal energy, the noise variance and the fading coefficients (or sufficiently accurate estimates) must be available to the receiver. Both of these metrics require full CSI.

A. Parameter Free Metrics

We will now develop decoder metrics that do not depend on E_s, N_0 or $a[k]$. Taylor series expansion of the Bessel function $I_0(\alpha)$ around zero yields

$$I_0(\alpha) = 1 + \frac{\alpha^2}{4} + O(\alpha^4) \quad (8)$$

which motivates the following approximation of the transition probabilities

$$p\left(\mathbf{y} \mid \mathbf{x} = \mathbf{e}_b\right) \approx 1 + \frac{E_s}{N_0^2} a^2 |y_b|^2 \quad (9)$$

and of the log-likelihood ratios (6),

$$\mathcal{L}(c[j(k,i)]) \approx \log \frac{\frac{M}{2} + \frac{E_s}{N_0^2} a[k]^2 \sum_{b \in \mathcal{B}_0^i} |y_b[k]|^2 q_{k,i}(b)}{\frac{M}{2} + \frac{E_s}{N_0^2} a[k]^2 \sum_{b \in \mathcal{B}_1^i} |y_b[k]|^2 q_{k,i}(b)}. \quad (10)$$

If we further assume that

$$\frac{E_{\rm s}}{N_0^2}a[k]^2\sum_{b\in\mathcal{B}_\omega^i}|y_b[k]|^2 \gg M/2 \tag{11}$$

for $\omega\in\{0,1\}$ we have

$$\mathcal{L}(c[j(k,i)]) \approx \log\frac{\sum_{b\in\mathcal{B}_0^i}|y_b[k]|^2 q_{k,i}(b)}{\sum_{b\in\mathcal{B}_1^i}|y_b[k]|^2 q_{k,i}(b)} \tag{12}$$

which is independent of $E_{\rm s}$, N_0 and the fading amplitudes $a[k]$. The interpretation of (12) is interesting. The receiver first measures the received energies at every frequency bin and computes the *empirical probability* at every bin as the fraction of the total received energy present in a given bin. Obviously, the normalization factor (the total energy $\sum_{i=0}^{M-1}|y_i[k]|^2$) cancels in (12).

We can further approximate (12) using the dual-max method as follows,

$$\begin{aligned}\mathcal{L}(c[j(k,i)]) \approx &\max_{b\in\mathcal{B}_0^i}\log(|y_b[k]|^2 q_{k,i}(b)) \\ &-\max_{b\in\mathcal{B}_1^i}\log(|y_b[k]|^2 q_{k,i}(b))\end{aligned} \tag{13}$$

which yields the corresponding parameter free dual-max metrics.

Equation (12) suggests the following definition of the parameter free transition probabilities as

$$p^\star(\mathbf{y}\mid\mathbf{x}=\mathbf{e}_b) = \frac{1}{\sum_{i=0}^{M-1}|y_i[k]|^2}|y_b[k]|^2. \tag{14}$$

By inserting (14) into (4) we get the parameter free mismatched information rate,

$$I^\star(X;Y) = \log_2 M - \mathbb{E}_{\mathbf{y}|\mathbf{x}=\mathbf{e}_0}\left[\log_2\left(1+\sum_{b=1}^{M-1}\Lambda_b^\star(\mathbf{y})\right)\right] \tag{15}$$

where

$$\Lambda_b^\star(\mathbf{y}) \triangleq \frac{|y_b|^2}{|y_0|^2}. \tag{16}$$

Remark that now $I^\star(X;Y)$ depends on $E_{\rm s}, N_0$ and a only through $\mathbf{y}$ and that $I^\star(X;Y)\le C$ by the data processing theorem [23]. Figure 2 also shows (dashed lines) the minimum $E_{\rm b}/N_0$ required for reliable communication with M-FSK with non-coherent detection in AWGN and Rayleigh fading using (15). In the AWGN case we observe that the optimal rate R is very close to that of the Bessel metrics. We also observe that the minimum $E_{\rm b}/N_0$ required to transmit very low rates is much higher. Also notice that in the AWGN case, the energy loss is small, while the Rayleigh fading case, the loss is larger, especially at low rates.

B. Numerical Examples

Before proceeding further, we present some numerical examples which demonstrate the utility of the parameter free metrics. Since we are interested in application of the metrics to iterative decoding, it is of interest to compare the corresponding EXIT charts [25].

Figure 3 shows EXIT charts for soft demodulation using the Bessel metrics (6) (solid), dual-max Bessel (7) (dashed), and the parameter free metrics (12) (dashed-dotted) and (13) (dotted). The charts are for 4-FSK, 16-FSK and 64-FSK modulation on the AWGN channel, Figure 3(a) and on the Rayleigh fading channel, Figure 3(b).

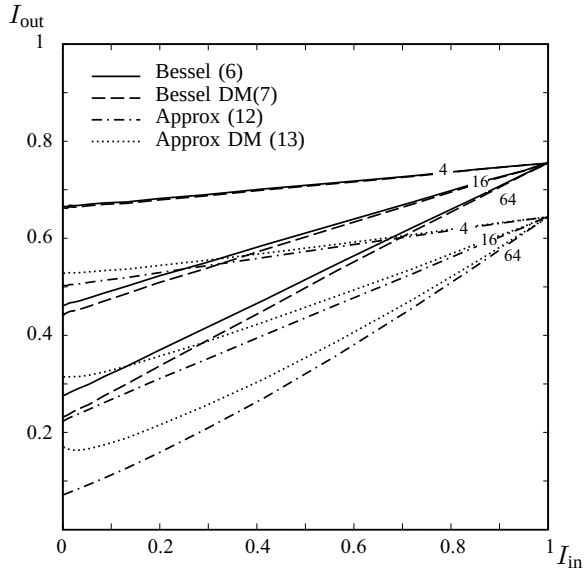

(a) AWGN

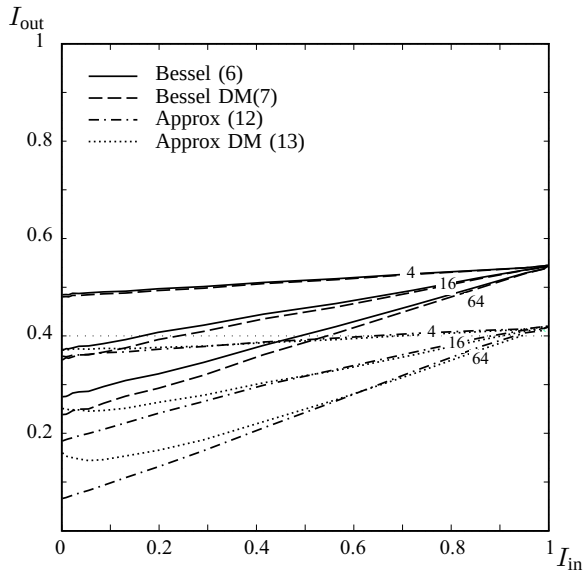

(b) Rayleigh Fading

Fig. 3. EXIT charts of the Bessel and parameter free metrics for 4, 16 and 64 NC-FSK on the AWGN (a) and Rayleigh fading (b) channel with $\gamma = 6$ dB.

The first observation is that the curves exhibit an almost-linear behavior, with Bessel metrics and parameter free metrics resulting in similar slopes. This implies that at higher γ, the parameter metrics will have the same EXIT chart, which will help in assessing the performance degradation due to the lack

of CSI.

Further, we observe that the parameter free metrics are information lossy, namely, when the input mutual information is $I_{\text{in}} = 1$, the output mutual information is lower than that obtained with Bessel metrics.

Finally, and perhaps most surprising, the parameter free dual-max metric (13) is significantly better than (12) at low I_{in}, despite the reduction in computational complexity. Application of the dual-max approximation following the Taylor approximation seems to regain some of the loss from the ideal Bessel metrics. As it will be illustrated in more detail later, this series of approximations induces a loss of Gaussianity in the iterative decoding process, which explains the slightly decreasing behavior of the curves for the metrics (13) for low I_{in}.

Figure 4(a) shows the demodulator EXIT charts for metrics (6), (12) and (13) at their respective SNR thresholds with the $(25, 27, 33, 37)_8$ convolutional code. Figure 4(b) shows the corresponding BER simulations with 10 decoding iterations and 10000 information bits per codeword. For the sake of clarity, we do not show the curves for the Bessel dual-max metrics (7), as the results are only slightly worse than the standard Bessel metrics (6). From Figure 4(b), it is apparent that as M grows, the error floor is pushed down to lower error rates, effectively disappearing for 64-FSK at BERs of practical interest. We also see that the metric (12) exhibits significant performance degradation with respect to its simpler dual max counterpart (13). The parameter free dual-max metrics (13) prove to be very robust and show performance close to the ideal Bessel metric. This result is quite remarkable, as the loss for not knowing the γ is shown to be around 0.6 dB.

Figures 5(a) and 5(b) show the EXIT charts and simulated trajectories for metrics (6) and (13) respectively. While, the EXIT analysis predicts the threshold behavior quite accurately for (6), the EXIT chart analysis is slightly pessimistic in the case of metrics (13) (see Figures 4(a) and 4(b) for reference with EXIT chart thresholds and real simulations). Furthermore, as we can see from Figure 5(b), the simulated decoding trajectories do not always follow the EXIT predictions. This is due to the fact that the Gaussian approximation inherent in the EXIT analysis is not accurate for mismatched decoder metrics. To illustrate this fact, Figures 5(c) and 5(d) show the empirical density evolution process. The solid lines represent the measured densities of the messages, while the dotted densities are Gaussian densities with the same extrinsic information rate. Iterations induce a left shift and larger variance on the distributions. As we observe, in the case of Bessel metrics, both density evolution and Gaussian approximation are very similar. On the other hand, in the case of the parameter free metrics (13) both are fairly different, which explains the divergence between true density evolution and the EXIT chart analysis (Gaussian approximation). Recall that metrics (13) are a result of three consecutive approximations to (6) and therefore, some loss in the Gaussianity of the iterative process is expected. However, as we have seen, the EXIT chart thresholds upperbound the true decoding thresholds, and the difference between the two is small.

Figure 6 shows the simulated bit-error rate for BICM with

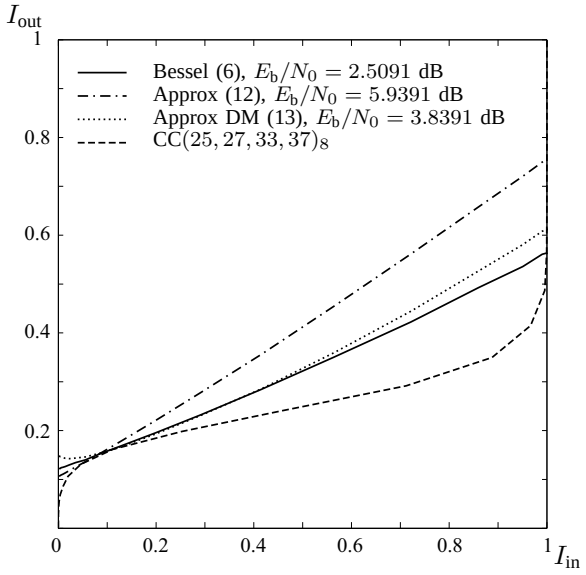

(a) EXIT charts for 64-ary NC-FSK. Each demodulator chart is shown at its E_b/N_0 threshold.

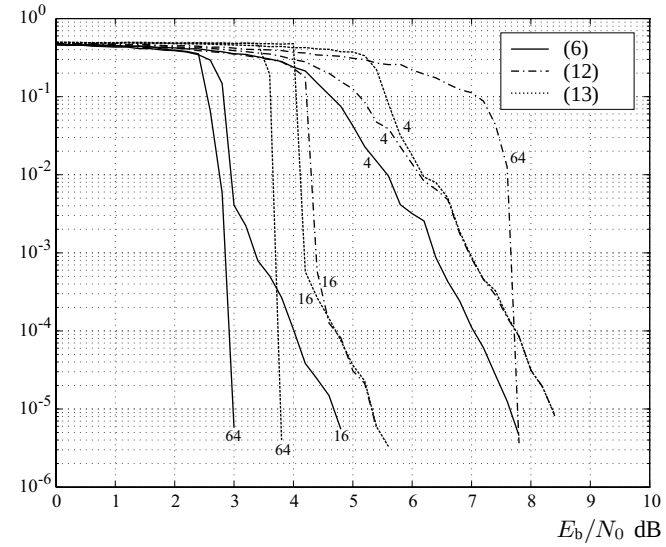

(b) Simulated BER results for 4, 16 and 64-ary NC-FSK.

Fig. 4. EXIT chart and BER results for BICM over the AWGN channel with a $(25, 27, 33, 37)_8$ outer convolutional code using Bessel (6) and parameter free metrics (12), (13).

an outer rate $R = 1/4$ repeat-accumulate code and 4, 16 and 64-ary NC-FSK. Figure 6(a) is for AWGN only, while Figure 6(b) is for Rayleigh fading. Metrics (6), (12) and (13) are considered.

The simulations were performed using $10,000$ information bits per codeword and 20 decoding iterations (one iteration of the RA decoder per demodulation iteration). Once again, the metrics (12) offer poor performance as M grows. In this case, the dual-max metric (13) pays a maximum penalty of only about 1.5 dB for not knowing E_s, N_0 or the fading amplitude.

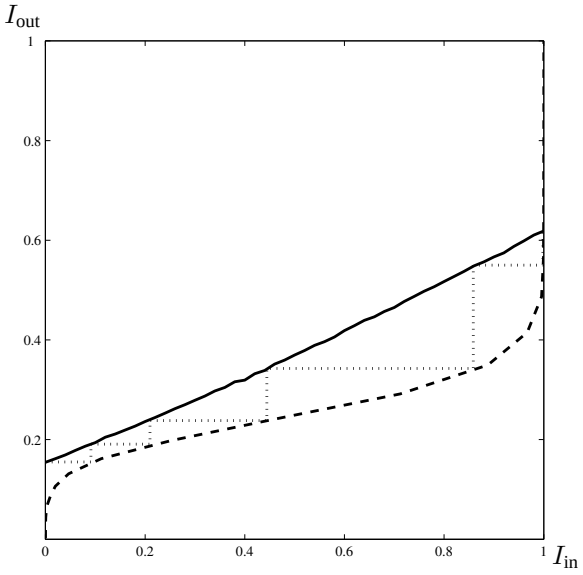

(a) Trajectory for 64-ary NC-FSK in AWGN with Bessel metrics (6) at $E_{\text{b}}/N_0 = 3$ dB.

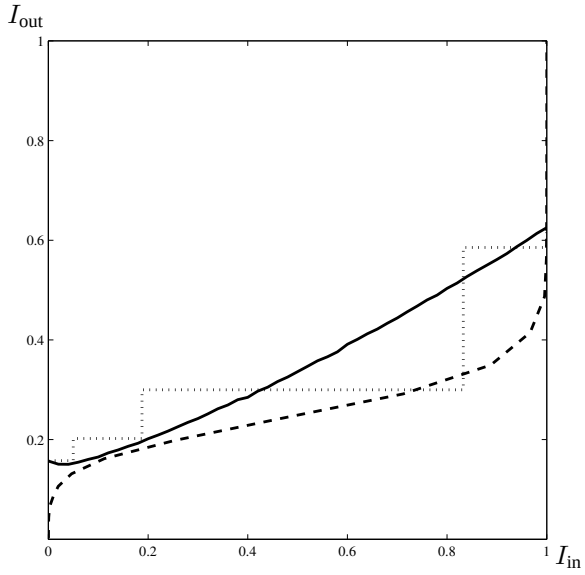

(b) Trajectory for 64-ary NC-FSK in AWGN with parameter free metrics (13) at $E_{\text{b}}/N_0 = 4$ dB.

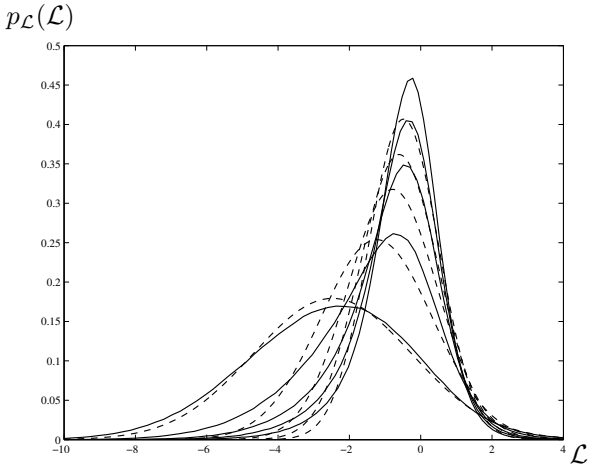

(c) Density evolution for 64-ary NC-FSK in AWGN with Bessel metrics (6) at $E_{\text{b}}/N_0 = 3$ dB.

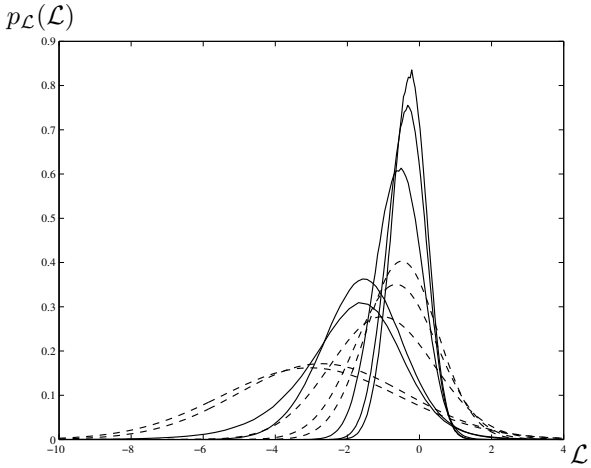

(d) Density evolution 64-ary NC-FSK in AWGN with parameter free metrics (13) at $E_{\text{b}}/N_0 = 4$ dB.

Fig. 5. EXIT chart trajectories and measured density evolution for BICM over the AWGN channel with a $(25, 27, 33, 37)_8$ outer convolutional code using Bessel (6) and parameter free metrics (13). Density evolution (solid lines) is compared to Gaussian distributions of the same extrinsic information rate (dashed lines). Iterations induce a left shift in the distributions.

V. Code Optimization

The results presented in the previous section were for BICM with an arbitrary selection of outer code (a similar approach was taken in [13], where an off-the-shelf code was considered). Our main intention however was to evaluate the utility of the parameter free metrics. In this section we proceed to optimize the choice of outer code, and consider more suitable modulation mappings.

Motivated by the serially concatenated coded modulation (SCCM) scheme of Tüchler [26], we particularize it to M-ary orthogonal modulation with outer irregular repetition codes. This approach consists of concatenating a binary outer code with a jointly designed inner code and modulator through a bit interleaver π. So we still have the system of Figure 1, where rather than use a memoryless modulator, we use a coded modulator with memory.

With reference to Figure 7, we propose an inner encoder/modulator that operates as follows. Encoding is performed on blocks of $2m$ bits. Pairs of bits from the block of $2m$ bits undergo a single parity check. The result is then encoded by a recursive rate m/m trellis code. The output of the recursive encoder is finally fed to the standard M-ary NC-FSK memoryless modulator (described above in Section IV). Thus the overall rate of the inner encoder/modulator is $2m$ bits per symbol.

Note that no interleaver is used between the encoder and the NC-FSK modulator, as suggested by [26]. An interesting characteristic of this inner code is that it reaches the $(1, 1)$ point on the EXIT chart [26]. The use of the single parity checks prior to trellis encoding further improves the proper-

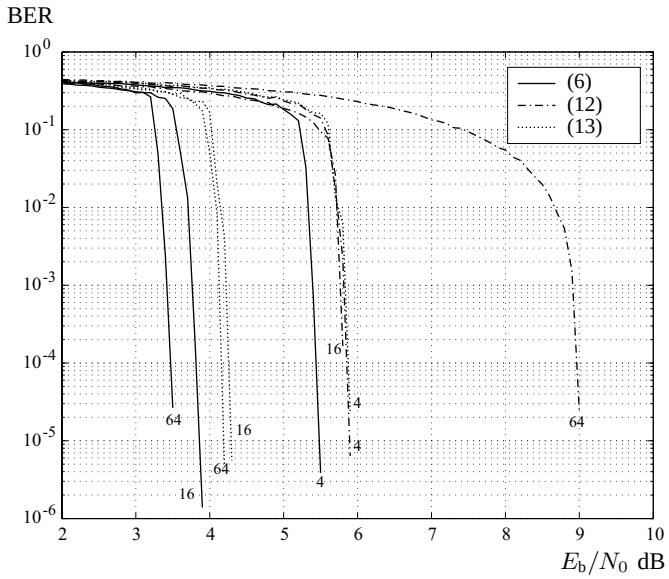

(a) AWGN channel.

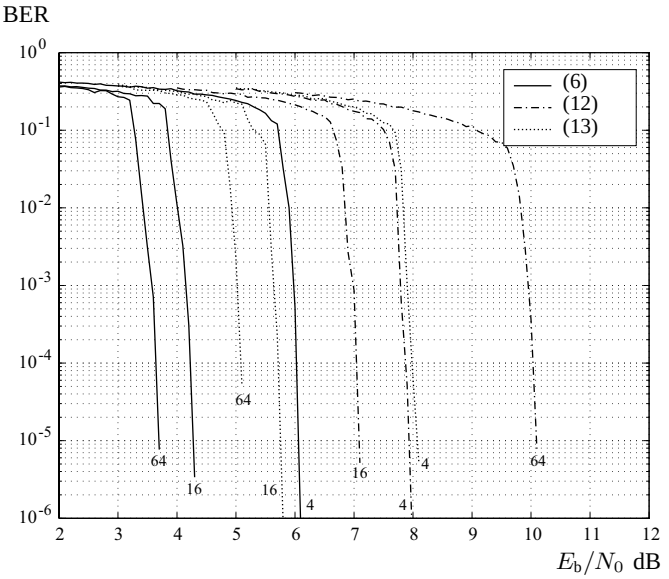

(b) Rayleigh fading channel.

Fig. 6. BER performance of BICM with outer rate $R = 1/4$ repeat accumulate code and 4, 16, 64 NC-FSK over AWGN and Rayleigh fading channel.

ties of the resulting EXIT charts, as discussed in [15]. The particular choice of trellis code shown in Figure 7 has been hand-selected for properties that are particularly convenient when it comes to optimizing the outer code.

For the outer code, we will use an irregular non-systematic repetition code of length n, defined by the degree distribution (edge perspective)

$$\left\{ \lambda_i \geq 0, i = 2, \ldots, d_{\max} : \sum_{i=2}^{d_{\max}} \lambda_i = 1 \right\},$$

where λ_i is the fraction of edges in the outer code graph connected to information bit nodes of degree i, and $d_{\max}$ is the maximum allowed degree (see [27] for details).

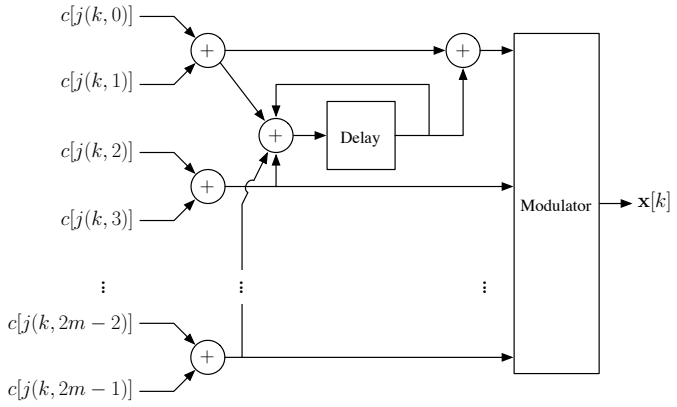

Fig. 7. Inner encoder/modulator for M-ary NC-FSK.

With these definitions, the number[1] of information bit nodes of degree i of the outer code is given by $k_i = \lambda_i n/i$ and the resulting code rate is

$$R = \frac{1}{n} \sum_{i=2}^{d_{\max}} k_i = \sum_{i=2}^{d_{\max}} \frac{\lambda_i}{i}.$$

The factor graph representation [28] of the overall serially concatenated code is shown in Figure 8. In our design, we do not use grouping nodes [27]. In a sense, the inner code nodes act as grouping nodes of grouping factor $2m$.

As shown in [14] for the binary erasure channel, the gap between capacity and the decoding threshold for iteratively decoded codes is related to the area between the EXIT charts of the outer and inner codes. This idea has been extensively used to optimize various irregular code ensembles over the AWGN [26], [15], [27]. In the AWGN channel, the area theorem [14] is not exact. For exact results the reader is referred to the generalized EXIT charts of [29]. Unfortunately, computing these generalized charts is not a simple task. However, codes resulting from optimization with standard EXIT charts are usually as close as desired from capacity (see e.g. [26], [15], [27]).

Let $I^I(u, \gamma)$ be the EXIT chart of the inner code at a given SNR γ and a priori mutual information u. Let $I_i^O(u)$ denote the EXIT chart of an outer regular repetition code of degree i. We can easily evaluate I_i^O in terms of the well-known J function [15] as follows,

$$I_i^O = J\left(J^{-1}(u)\sqrt{i-1}\right), \tag{17}$$

where

$$J(x) = 1 - \int \frac{e^{-(t-x^2/2)}/2x^2}{\sqrt{2\pi x^2}} \log_2(1+e^{-t})dt. \tag{18}$$

Accurate numerical evaluation of $J(x)$ and $J^{-1}(x)$ is possible using the approximations in [16].

Finally, the EXIT chart of an irregular repetition code is simply the weighted sum of the degree-i charts [14], [15],

[1] In practice, some small adjustments are required to ensure that the k_i are integer.

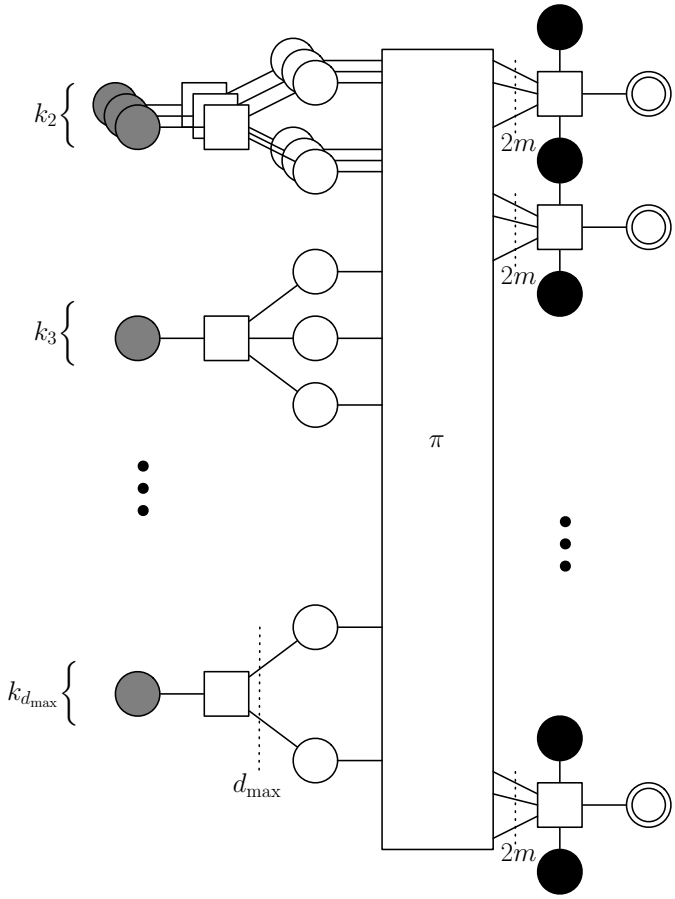

Fig. 8. Factor graph representation of the entire code. Grey circles denote the message bits, the white circles denote the outer coded bits, double circles denote the M-ary symbols, black circles represent the inner code state. Squares represent the encoding constraint functions.

[16]

$$I^O = \sum_{i=1}^{d_{\max}} \lambda_i I_i^O.$$

We can therefore use linear programming to optimize the outer code degree distribution, to minimize the area between the inner and outer code EXIT charts [15], [27]. Figure 9 shows the results of this curve fitting procedure for 8-ary modulation with rate $1/2$ codes.

Tables I and II summarize the results of our code search for the AWGN and Rayleigh fading channels. There are two main conclusions. First, we have found codes very close to capacity, ranging from 0.4 - 0.05 dB in the case of Bessel metrics. Smaller gaps are possible by using larger (and eventually irregular) grouping factors [15], [27]. This can be compared to gaps of 0.9 - 1.7 dB reported in [13], where no code optimization was performed. Secondly, the maximum degree for the optimized codes is not unrealistically high. In our linear program we allowed much higher $d_{\max}$ (up to 50), but fortuitously such high degree nodes were not required. These low maximum degrees, coupled with the extremely simple inner code results in a system with very low implementation complexity.

Figure 10 shows simulated BER results for the optimized

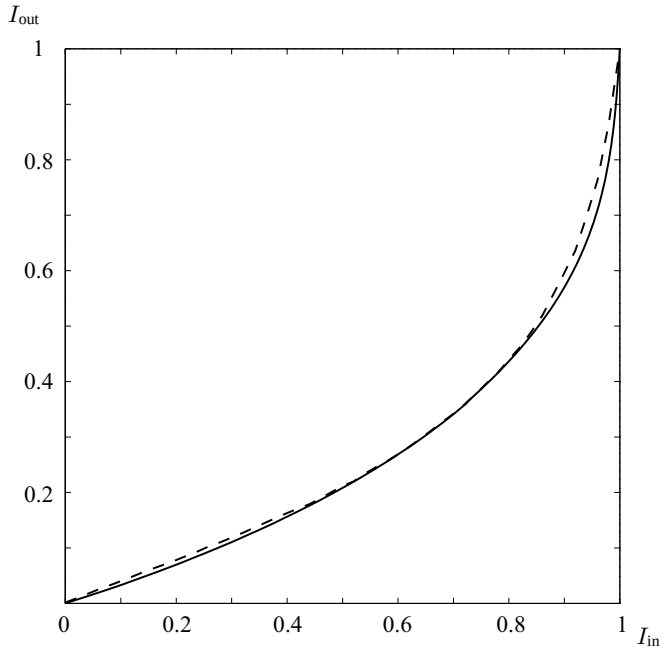

Fig. 9. EXIT charts of optimized 8-ary NC-FSK coded modulation with $R = 1/2$ at its threshold ($E_{\text{b}}/N_0 = 3.039$ dB) in the AWGN channel. Solid line is the outer code. Dashed line is the inner coded modulator

rate $1/2$ codes with 8 NC-FSK the AWGN channel, along with capacity (solid) and the predicted decoding threshold (dashed) for Bessel and dual-max parameter free metrics. The capacity values for Bessel and parameter free metrics are very close to each other (see Table I for the exact values). A block length of $150,000$ was used for the simulation with 100 decoding iterations. Once again, in the case of the Bessel metrics, the simulated and curve-fitting EXIT results match very well. In the case of the dual-max parameter free metrics the simulation is slightly better than the EXIT analysis threshold, as for the case of memoryless BICM, due to the EXIT trajectory inaccuracy.

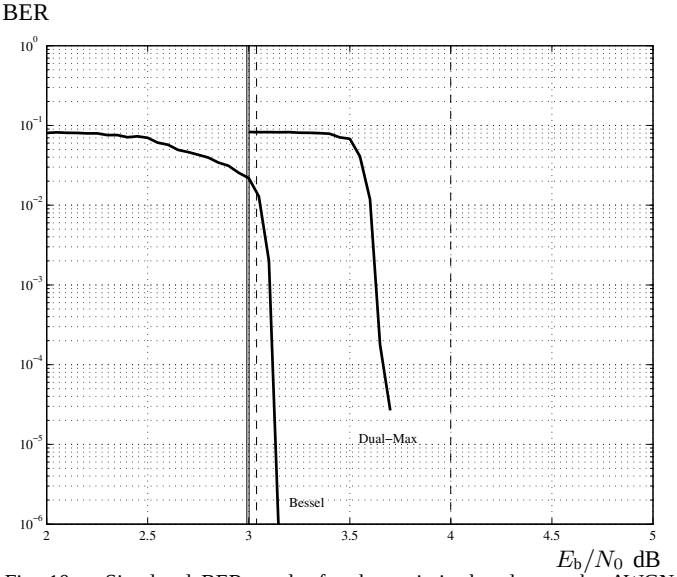

Fig. 10. Simulated BER results for the optimized codes on the AWGN channel.

TABLE I

OPTIMAL CODES FOR $M = 4, 8, 16$ AND 64 IN THE AWGN CHANNEL WITH BESSEL AND PARAMETER FREE METRICS. (*) INDICATES DUAL-MAX.

M	R	Bessel Metrics			Parameter Free Metrics		
		Capacity	Threshold	Distribution	Information Rate	Threshold	Distribution
4	1/4	4.6172 dB	4.7602 dB	$\lambda_2 = 0.0483$ $\lambda_4 = 0.1250$ $\lambda_{11} = 0.0911$ $\lambda_{12} = 0.7356$	4.8920 dB	5.2103 dB	$\lambda_2 = 0.0213$ $\lambda_3 = 0.1173$ $\lambda_{11} = 0.4567$ $\lambda_{12} = 0.4047$
	1/2	4.1809 dB	4.3500 dB	$\lambda_2 = 0.1413$ $\lambda_4 = 0.1523$ $\lambda_5 = 0.7064$	4.2723 dB	* 5.0750 dB	$\lambda_2 = 0.0845$ $\lambda_4 = 0.4933$ $\lambda_5 = 0.4223$
8	1/4	3.5484 dB	3.5994 dB	$\lambda_2 = 0.0193$ $\lambda_4 = 0.1152$ $\lambda_{10} = 0.8655$	3.6123 dB	3.9494 dB	$\lambda_2 = 0.0585$ $\lambda_9 = 0.1455$ $\lambda_{10} = 0.7960$
	1/2	2.9904 dB	3.0391 dB	$\lambda_2 = 0.0581$ $\lambda_4 = 0.6512$ $\lambda_5 = 0.2907$	3.0015 dB	* 3.9991 dB	$\lambda_2 = 0.1244$ $\lambda_4 = 0.2536$ $\lambda_5 = 0.6220$
16	1/4	2.5921 dB	2.600 dB	$\lambda_2 = 0.042017$ $\lambda_4 = 0.0442165$ $\lambda_5 = 0.151857$ $\lambda_{12} = 0.617372$ $\lambda_{13} = 0.1445366$	2.8389 dB	3.2 dB	$\lambda_2 = 0.0485$ $\lambda_5 = 0.0816$ $\lambda_7 = 0.3099$ $\lambda_{11} = 0.3488$ $\lambda_{25} = 0.2112$
	1/2	2.0685 dB	2.1397 dB	$\lambda_2 = 0.128628$ $\lambda_4 = 0.255314$ $\lambda_5 = 0.575429$ $\lambda_6 = 0.040627$	2.1574 dB	* 3.4397 dB	$\lambda_2 = 0.1030$ $\lambda_3 = 0.1939$ $\lambda_4 = 0.0254$ $\lambda_5 = 0.4376$ $\lambda_6 = 0.2402$
64	1/4	1.6845 dB	1.6890 dB	$\lambda_2 = 0.04975$ $\lambda_6 = 0.163822$ $\lambda_7 = 0.425504$ $\lambda_{30} = 0.36091$	1.9289 dB	2.6391 dB	$\lambda_2 = 0.0437$ $\lambda_5 = 0.2186$ $\lambda_6 = 0.2612$ $\lambda_{30} = 0.4765$
	1/2	1.1155 dB	1.1487 dB	$\lambda_2 = 0.114061$ $\lambda_3 = 0.156532$ $\lambda_4 = 0.463261$ $\lambda_{10} = 0.085959$ $\lambda_{11} = 0.180176$	1.1980 dB	* 3.4288 dB	$\lambda_2 = 0.1223$ $\lambda_3 = 0.2276$ $\lambda_4 = 0.1877$ $\lambda_7 = 0.4624$

TABLE II

OPTIMAL CODES FOR $M = 4, 8, 16$ AND 64 IN THE RAYLEIGH FADING CHANNEL WITH BESSEL AND PARAMETER FREE METRICS. (*) INDICATES DUAL-MAX.

M	R	Bessel Metrics			Parameter Free Metrics		
		Capacity	Threshold	Distribution	Information Rate	Threshold	Distribution
4	1/4	4.8758 dB	5.1103 dB	$\lambda_2 = 0.0333$ $\lambda_4 = 0.1007$ $\lambda_{11} = 0.3431$ $\lambda_{12} = 0.5229$	6.0841 dB	7.1103 dB	$\lambda_2 = 0.0583$ $\lambda_9 = 0.1520$ $\lambda_{10} = 0.7897$
	1/2	5.7865 dB	6.1000 dB	$\lambda_2 = 0.1459$ $\lambda_4 = 0.1247$ $\lambda_5 = 0.7294$	6.3845 dB	8.300 dB	$\lambda_2 = 0.0911$ $\lambda_4 = 0.4532$ $\lambda_5 = 0.4557$
8	1/4	3.5661 dB	3.9494 dB	$\lambda_2 = 0.0550$ $\lambda_9 = 0.2697$ $\lambda_{10} = 0.6753$	4.6596 dB	5.7494 dB	$\lambda_2 = 0.0505$ $\lambda_9 = 0.4303$ $\lambda_{10} = 0.5191$
	1/2	4.4773 dB	4.9391 dB	$\lambda_2 = 0.1113$ $\lambda_4 = 0.3321$ $\lambda_5 = 0.5566$	5.0739 dB	* 7.3391 dB	$\lambda_2 = 0.0639$ $\lambda_4 = 0.6164$ $\lambda_5 = 0.3196$
16	1/4	2.7831 dB	3.050 dB	$\lambda_2 = 0.0533$ $\lambda_9 = 0.3311$ $\lambda_{10} = 0.6156$	3.8839 dB	5.0000 dB	$\lambda_2 = 0.0416$ $\lambda_9 = 0.7528$ $\lambda_{10} = 0.2056$
	1/2	3.6292 dB	4.1397 dB	$\lambda_2 = 0.0017$ $\lambda_4 = 0.9898$ $\lambda_5 = 0.0085$	4.2166 dB	* 6.7897 dB	$\lambda_2 = 0.0806$ $\lambda_4 = 0.5364$ $\lambda_5 = 0.3830$
64	1/4	1.8461 dB	1.9391 dB	$\lambda_2 = 0.0455$ $\lambda_9 = 0.6107$ $\lambda_{10} = 0.3438$	2.8610 dB	4.2391 dB	$\lambda_2 = 0.0440$ $\lambda_6 = 0.0015$ $\lambda_7 = 0.5818$ $\lambda_{19} = 0.3726$
	1/2	2.6387 dB	2.9788 dB	$\lambda_4 = 1$	3.2099 dB	* 6.2288 dB	$\lambda_2 = 0.0944$ $\lambda_4 = 0.4339$ $\lambda_5 = 0.4718$

VI. Conclusions

We have found a low complexity method of computing metrics suited for iterative demodulation/decoding of M-ary non-coherent orthogonal modulation that does not require any knowledge of the signal-to-noise ratio or fading coefficients at the receiver. The method is based on the first-order Taylor series expansion of the Bessel function and dual-max approximation. The proposed method performs very close of the ideal metrics. This enables the use of methods such as bit-interleaved coded modulation over non-coherent channels without side information. We have also designed new codes for the $4, 8, 16$ and 64-ary non-coherent orthogonal modulation channel. These codes are a concatenation of an irregular repeat code and an two-state trellis coded modulator. By optimizing the degree sequence of the outer code we have found codes with decoding thresholds within 0.15 dB of capacity, surpassing all previously known codes. Furthermore, the optimized codes are very low complexity, with low maximum degree.

References

[1] W. E. Stark, "Capacity and cutoff rate of noncoherent FSK with nonselective Rician fading," *IEEE Trans. Commun.*, vol. 33, pp. 1153–1159, Nov. 1985.

[2] C. D. Frank and M. B. Pursley, "Concetenated coding for frequency-hop spread-spectrum with partial-band interference," *IEEE Trans. Commun.*, vol. 44, no. 3, pp. 377–387, Mar. 1996.

[3] S. Kim and W. E. Stark, "Performance limits of Reed-Solomon coded CDMA with orthogonal signaling in a Rayleigh-fading channel," *IEEE Trans. Commun.*, vol. 46, pp. 1125–1134, Sept. 1998.

[4] M. Chu and W. E. Stark, "Asymptotic performance of a coded communication system with orthogonal signaling in partial band jamming," in *IEEE Military Communications Conference*, 1998, pp. 1003–1007.

[5] J. D. Choi, D.-S. Yoo, and W. E. Stark, "Performance limits of m-FSK with Reed-Solomon coding and diversity combining," *IEEE Trans. Commun.*, vol. 50, no. 11, pp. 1787–1797, Nov. 2002.

[6] G. Garrabrant and J. Ehrenberg, "Trellis coded modulation applied to noncoherent detection of orthogonal signals," in *IEEE Military Communications Conference*, Oct. 1989, pp. 774–778.

[7] J. Vainappel, E. Hardy, and D Raphaeli, "Noncoherent turbo decoding," in *IEEE Global Communications Conf.*, San Antonio, USA, Nov. 2001, pp. 952–956.

[8] A. Ramesh, A. Chockalingham, and L. B. Milstein, "Performance of noncoherent turbo detection on Rayleigh fading channels," in *IEEE Global Communications Conf.*, San Antonio, USA, Nov. 2001, pp. 1193–1198.

[9] X. Li and J. A. Ritcey, "Trellis-coded modulation with bit interleaving and iterative decoding," *IEEE J. Select. Areas Commun.*, pp. 715–724, April 1999.

[10] G. Caire, G. Taricco, and E. Biglieri, "Bit-interleaved coded modulation," *IEEE Trans. Inf. Theory*, vol. 44, no. 3, pp. 927–946, May 1998.

[11] S. Cheng and M.C. Valenti, "Bit-interleaved turbo-coded noncoherent orthogonal modulation with iterative demodulation and decoding: Capacity limits and convergence analysis," in *Thirty-Eighth Asilomar Conference on Signals, Systems and Computers*, Nov. 2004, pp. 2020–2024.

[12] M. C. Valenti, E. Hueffmeier, B. Bogusch, and J. Fryer, "Towards the capacity of noncoherent orthogonal modulation: BICM-ID for turbo coded NFSK," in *IEEE Military Communications Conference*, 2004, pp. 1549–1555.

[13] M. C. Valenti and S. Cheng, "Iterative demodulation and decoding of turbo-coded M-ary noncoherent orthogonal modulation," *IEEE J. Select. Areas Commun. (Special Issue on Differential and Noncoherent Wireless Communications)*, vol. 23, no. 9, pp. 1739–1747, Sept. 2005.

[14] A. Ashikhmin, G. Kramer, and S. ten Brink, "Extrinsic information transfer functions: model and erasure channel properties," *IEEE Trans. Inf. Theory*, vol. 50, no. 11, pp. 2657–2673, Nov. 2004.

[15] S. ten Brink and G. Kramer, "Design of repeat accumulate codes for iterative detection and decoding," *IEEE Trans. Sig. Proc.*, vol. 51, no. 11, pp. 2764–2772, Nov. 2003.

[16] S. ten Brink, G. Kramer, and A. Ashikhmin, "Design of low-density parity-check codes for modulation and detection," *IEEE Trans. Commun.*, vol. 52, no. 4, pp. 670–678, April 2004.

[17] H. Jin, A. Khandekar and R. McEliece, "Irregular repeat-accumulate codes," in *2nd International Symposium on Turbo Codes and Related Topics, Brest, France*, Sept. 2000.

[18] J. Proakis, *Digital Communications*, McGraw-Hill, 1995.

[19] M. Abramowitz and I. A. Stegun, *Handbook of Mathematical Functions with Formulas, Graphs and Mathematical Tables*, New York: Dover Press, 1972.

[20] W. H. Press, S. A. Teukolsky, W. T. Vetterling and B. P. Flannery, *Numerical Recepies in C*, 2nd Ed., Cambridge University Press, also available at `http://www.nr.com`, 1992.

[21] T. R. M. Fisher "Some remarks on the role of inaccuracy in Shannon's theory of information transmission," in *Trans. 8th Prag. Conf. Inform. Theory*, 1978, pp 211-226.

[22] N. Merhav, G. Kaplan, A. Lapidoth, and S. Shamai, "On information rates for mismatched decoders," *IEEE Trans. Inf. Theory*, vol. 40, pp. 1953-1967, Nov. 1994.

[23] T. M. Cover and J. A. Thomas, *Elements of Information Theory*, Wiley Series in Telecommunications, 1991.

[24] C. Berrou, A. Glavieux and P. Thitimajshima, "Near Shannon limit error correcting coding and decoding: Turbo codes," in *Proc. IEEE Int. Conference on Communications, Geneva, Switzerland*, 1993.

[25] S. ten Brink, "Designing iterative decoding schemes with the extrinsic information transfer chart," *AEU Int. J. Electron. Commun.*, vol. 54, no. 6, pp. 389–398, Dec. 2000.

[26] M. Tuechler, "Design of serially concatenated systems depending on the block length," *IEEE Trans. Commun.*, vol. 52, no. 2, pp. 209–218, Feb. 2004.

[27] A. Roumy, S. Guemghar, G. Caire and S. Verdú, "Design methods for irregular repeat-accumulate codes," *IEEE Trans. Inf. Theory*, vol. 50, no. 8, pp. 1711–1727, Aug. 2004.

[28] F. R. Kschischang, B. J. Frey, and H-A. Loeliger, "Factor graphs and the sum-product algorithm," *IEEE Trans. Inf. Theory*, vol. 47, no. 2, pp. 498–519, Feb. 2001.

[29] A. Montanari C. Méasson and R. Urbanke, "Why we can not surpass capacity: The matching condition," *43rd Allerton Conference on Communication, Control and Computing*, Sept. 2005.

PLACE PHOTO HERE

Albert Guillén i Fàbregas (S '01 – M '05) was born in Barcelona, Catalunya, Spain, in 1974. He received the Telecommunication Engineering Degree and the Electronics Engineering Degree from Universitat Politècnica de Catalunya, Barcelona, Catalunya, Spain, and the Politecnico di Torino, Torino, Italy, respectively, in 1999, and the Ph.D. in Communication Systems from Ecole Polytechnique Fédérale de Lausanne (EPFL), Lausanne, Switzerland, in 2004.

From August 1998 to March 1999, he conducted his Final Research Project at the New Jersey Institute of Technology, Newark, NJ. He was with Telecom Italia Laboratories, Italy, from November 1999 to June 2000 and with the European Space Agency (ESA), Noordwijk, The Netherlands from September 2000 to May 2001. During his doctoral studies, from 2001 to 2004, he was a Research and Teaching assistant at the Mobile Communications Department, Institut Eurécom, Sophia-Antipolis, France. From June 2003 to July 2004 he was a visiting scholar at the Communications Theory Lab at EPFL. From September 2004 to December 2006 he was a Research Fellow at the Institute for Telecommunications Research, University of South Australia, Mawson Lakes, Australia. During June-July 2005 and June 2006 he held a visiting appointment at Ecole Nationale Supérieure des Télécommunications, Paris, France. Since 2007 he has been a Lecturer at the Department of Engineering, University of Cambridge, Cambridge, UK. His specific research interests are in the area of communication theory, information theory, coding theory, digital modulation and signal processing techniques, particularly with wireless terrestial and satellite applications.

Dr. Guillén i Fàbregas received a pre-doctoral Research Fellowship of the Spanish Ministry of Education to join ESA. He received the Young Authors Award of the 2004 European Signal Processing Conference EUSIPCO 2004, Vienna, Austria and the 2004 Nokia Best Doctoral Thesis Award in Mobile Internet and 3rd Generation Mobile Solutions from the Spanish Institution of Telecommunications Engineers. He is also a member of the ARC Communications Research Network (ACoRN).

PLACE PHOTO HERE

Alex J. Grant (S '93 – M '96 – SM '03) received the B.E. and Ph.D. degrees from the University of South Australia, Mawson Lakes, Australia, in 1993 and 1996, respectively.

In 1997, he was a Postdoctoral Research Fellow at the Laboratory for Signal and Information Processing, ETH Zürich, Zürich, Switzerland. Since March 1998, he has been with the Institute for Telecommunication Research, University of South Australia, where he is now Research Professor of Information Theory. His research interests include information theory and its applications to multiple user and other communications problems.

Prof. Grant served as Chairman for the IEEE SA/ACT/Vic Sections Information Theory Society Joint Chapter (2000–2003). He served as Technical Co-Chair for the 2001 IEEE Information Theory Workshop and as general Co-Chair for the 2005 IEEE International Symposium on Information Theory, Adelaide, Australia. He is a Member of the Board of Governors of the IEEE Information Theory Society and is an Associate Editor for the IEEE TRANSACTIONS ON WIRELESS COMMUNICATIONS.